Trans Indian Inst Met (2024) 77(4):1025–1038
https://doi.org/10.1007/s12666-023-03176-w

ORIGINAL ARTICLE

Effect of Forge-Time on Electrode Indentation, Thermal and Residual Stress Fields in Resistance Spot Weld Joints of AISI 1008 Steel Sheets

Prashanth Kumar Reddy Gillela[1] · Jeevan Jaidi[1] · Venugopal Gude[2] · Sunil Kumar Pathak[2] · Sudipta Pramanik[2]

Received: 29 November 2022 / Accepted: 9 November 2023 / Published online: 3 January 2024

Abstract Resistance spot welding is extensively used in automotive, aerospace, electronics and nuclear industries owing to its ease of automation and economy. However, the stability of a welded structure depends on the joint strength, which in turn depends on the nugget size and residual stresses across the nugget. In the present simulations-based study, the effect of forge (hold) time on electrode displacement, sheet metal deformation and residual stresses is being explored and discussed. 2D axisymmetric fully coupled phenomena model is developed in COMSOL software by considering the elastoplasticity of sheet metals and temperature dependent properties of sheet and electrode materials. Contact conductance model for resistances to the transport phenomena across the interfaces and apparent heat capacity model for phase change (melting and solidification) effects are used. For the selected process parameters (load, current and time), a close agreement is found between the predicted and measured nugget diameter. Also, it is found that increasing the forge time has lowered the residual stresses below the yield stress and a transition from tensile to compressive stresses in the heat-affected zone. Further, the coupled model predicted the minimum forge (hold) time required for an electrode indentation on the sheets, which signifies the nugget zone.

Keywords Contact conductance · Nugget diameter · Forge time · Electrode indentation · Residual stress

✉ Jeevan Jaidi
jaidi@hyderabad.bits-pilani.ac.in

[1] Department of Mechanical Engineering, BITS Pilani, Hyderabad, Telangana 500078, India

[2] Nuclear Fuel Complex, Hyderabad, Telangana 500062, India

List of Symbols

c	4th order elastic tensor, in Eq. 9
C_p	Specific heat, kJ/kg.K
ECC	Electrical contact conductance, S/m^2
J	Current density, A/m^2
k	Thermal conductivity, W/m.K
L	Latent heat, kJ/kg
Q_e	Volumetric heat generation rate, W/m^3
$\dot{q}''$	Heat flux, W/m^2
S	Stress in Hook's law, Pa
S_0	Initial stress, Pa
t	Time, s
T	Temperature, K
TCC	Thermal contact conductance, W/m^2.K
u	Displacement, m

Greek Symbols

ρ	Mass density, kg/m^3
α	Coefficient of thermal expansion, K^{-1}
V	Electric potential, V
θ_1	Fraction of solid phase 1
θ_2	Fraction of liquid phase 2
α_m	Mass fraction
σ	Electrical conductivity, S/m
ε	Engineering strain tensor
ε_o	Initial strain
ε_{inel}	Inelastic strain
∇u	Displacement gradient

Subscripts and Superscripts

°	Degree
e	Electrical
:	Double-dot tensor product
T	Transpose

1 Introduction

Resistance spot welding (RSW) process is widely used in automotive and aerospace industries to join thin sheets of ferrous and non-ferrous similar and dissimilar metals. The strength of a welded joint depends on the nugget diameter as well as the magnitude of residual stresses. For maximum joint strength, the nugget diameter must be large with minimum residual stresses. Since the precise measurements in the nugget region is highly difficult, numerical simulations using a multiphysics coupled model can be very handy and predict the nugget diameter and residual stresses in a cost-effective way. The RSW process consists of squeeze, weld and hold stages. During the squeeze stage, load is applied through the electrodes to provide good contact at the electrode-workpiece and workpiece-workpiece interfaces. Subsequently, in the weld stage, current is passed across the sheets through the electrodes. Due to bulk and contact resistances, the sheets are heated and form a nugget (molten region) between the sheets. Further, in the hold stage, current is cut-off and sheets are still under the electrode load. Since the copper-alloy electrodes are highly conductive and water-cooled, the molten nugget solidifies rapidly. Finally, the sheets are unloaded and cooled in ambient air. It can be noted that during the weld stage (heating period), the sheets develop compressive stresses, while tensile stresses during the hold stage (cooling period). Therefore, the magnitude of residual stresses primarily depends on the heating and cooling rates, the peak temperature as well as the forge (hold) time.

Pouranvari [1] experimentally studied the mechanical properties and failure mode of the RSW joints of HSLA 420 steel sheets and suggested that the pullout failure mode is preferred over the interfacial failure mode because of higher plastic deformation and energy absorption. The authors proposed an empirical equation for the minimum nugget diameter to achieve a pullout failure. Mirzaei et al. [2] measured the nugget dimensions and tensile shear strength of the RSWed joints of galvanized interstitial-free (IF) and bake hardened steels. The authors stated that the failure occurs in a region where the von Mises stress exceeds the ultimate stress of the weldment. Rao et al. [3] used the artificial neural networks (ANN) method to optimize the process parameters for the RSW joints of DP 590 steel, and found that increasing the heat input increases the joint strength (tensile shear and coach-peel tests) and then decreases due to molten metal expulsion. Aydin et al. [4] studied the effect of current on hardness, microstructures and shear strength (tensile and cross-tensile tests) of dissimilar RSW joints of DP 600 and 800 steel sheets. The authors found that the shear strength increases with increasing the current and then decreases due to molten metal expulsion. Raath et al. [5] measured hardness and residual stresses in boron steel and DP 600 steel sheets, and found tensile stresses in the nugget and compressive stresses in the HAZ. Ao et al. [6] measured the residual stresses in stainless steel sheets and found compressive stresses in the nugget center and tensile stresses at its edge. Also, the residual stresses on sheet surface are tensile with maximum value at the center and decreases away from it.

Gould [7] developed a 1D finite-difference model with the assumption of uniform current density and constant contact resistances, and found the predicted nugget size of AISI 1008 steel sheets larger than the measured one. Tsai et al. [8] developed a 2D axisymmetric model (in ANSYS software) considering the temperature dependent electrical resistivity, and predicted the electrode displacement during the RSW process. Gupta and De [9] developed a 2D model and simulated the RSW process of low-carbon steel and HSLA steel sheets. The authors observed a close match between the predicted and measured thermal cycles and nugget size. Babu et al. [10] proposed an analytical equation for the contact resistance as a function of temperature and pressure, and concluded that it is a strong function of temperature. A 2-D axisymmetric model by De [11] considered the elastoplasticity and temperature dependent properties of Al-alloy sheets, and predicted the nugget diameter and thermal cycles. Hou et al. [12] modeled the contact pressure variation and found maximum compressive stress at the edge of electrode-workpiece interface during the squeeze stage and also at the edge of nugget during the weld stage. Moshayedi et al. [13] developed a 2D axisymmetric model for the RSW process of AISI 304 steel sheets and investigated the contact pressure variation and stresses across the nugget. Wang et al. [14] investigated the effect of electrode morphologies on the RSW quality of DP 590 steel and found that increase in pitting and electrode tip diameter result in loss of weld strength. Lee et al. [15] used a 3D model in ABAQUS software and studied the nugget size and stress distribution of SPRC 340 steel sheets. The authors found the compressive stresses in the nugget center and tensile stresses at its edge during the weld stage. A detailed review on available contact resistance models for the RSW process was discussed by Hamedi et al. [16]. The authors concluded that in order to develop an efficient contact resistance model, it is necessary to mathematically characterize the constriction resistance. Guan et al. [17] used the electromagnetic-acoustic model in COMSOL software and evaluated the nugget diameter and indentation depth, and found a good agreement with the measured data. Chino et al. [18] used an inherent strain method to predict the sheet deformation and observed three different deformation modes (in-plane shrinkage, out-of-plane shrinkage and out-of-plane bending), and found a close match with the measurements. Brizes et al. [19] modeled the RSW process using different simulation softwares and studied the nugget diameter and electrode displacement. The authors observed that the predictions by the ABAQUS

software are in close agreement with the measured data than by the SORPAS software. Recently, the present authors (Gillela et al. [20]) developed a 2D axisymmetric coupled electrothermal–mechanical model for the RSW of AISI 1008 steel sheets and studied the effect of weld current and time on the nugget size. The authors concluded that the nugget diameter grow faster than the penetration.

Nodeh et al. [21] used an electrothermal–mechanical coupled model and predicted the residual stresses in the RSW of steel sheets. Also, the authors measured the residual stresses on the sheet surface, and found tensile stress at the center and compressive at the edge of indentation. Dalewski et al. [22] performed simulations and experiments to study the residual stresses and microstructures in the RSW of steel sheets. The authors found a good agreement between the predicted and measured tensile shear strength. Iyota et al. [23] numerically studied the effect of electrode load on nugget diameter and residual stresses in HSLA steel sheets, and found that a decrease in load during the weld stage results in increased nugget diameter. Further, an increase in load during the hold stage decreases the tensile residual stresses. Wan et al. [24] investigated on the contact pressure, deformation and flow stress distribution in DP 600 steel sheets and observed compressive stresses in the nugget and tensile stresses at its edge at the end of hold stage. Moharrami et al. [25] developed a 3D finite element model and investigated the stress distribution across the nugget at different stages of the RSW process, and found the maximum tensile residual stress at the nugget edge. Prabitz et al. [26] developed a multiphysics model in ABAQUS software for the RSW process of DP 1200 HD steel sheets and studied the stresses and strains. The predicted residual stresses along the radial and tangential directions are in agreement with the measured data. A review on different numerical models and experimental techniques used by researchers to study the residual stresses in the RSW process are discussed by Khanna et al. [27] and De and Debroy [28].

From the above detailed literature summary, it can be found that only a few researchers have done simulations considering the forge (hold) stage to predict the residual stresses and electrode indentation. Also, literature is not available on the effect of forge time on the magnitude of residual stresses. The present work is an extension of the authors' recent work [20] and now considered the elastoplastic behavior of AISI 1008 steel sheets to investigate the effect of different forge times on the evolution of residual stresses, electrode indentation and workpiece deformation.

2 Mathematical and Numerical Modelling

In this section, the governing equations pertaining to different phenomena involved in RSW process are discussed first, followed by the numerical models used in the present simulations.

2.1 Governing Equations

In RSW process, different phenomena involved such as electrical, thermal, mechanical and metallurgy are simultaneously acting and are strongly coupled.

2.1.1 Electrical Phenomenon

Current density is governed by,

$$\mathrm{J} = -\sigma \nabla V \tag{1}$$

Current continuity is given by,

$$\nabla \cdot J = 0 \tag{2}$$

Resistive heating due to electric current is given by,

$$Q_e = J \cdot E \tag{3}$$

2.1.2 Thermal Phenomenon

The energy equation is given by,

$$\rho C_P \frac{\partial T}{\partial t} + \nabla .q = Q_e \tag{4}$$

The phase change is modelled using Latent heat capacity method [29]

$$C_P = \theta_1 C_{p1} + \theta_2 C_{P2} + L \frac{\partial \alpha_m}{\partial t} \tag{5}$$

$$\alpha_m = \frac{1}{2} \frac{\theta_1 \_ \theta_2}{\theta_1 + \theta_2} \tag{6}$$

$$\theta_1 + \theta_2 = 1 \tag{7}$$

2.1.3 Mechanical Phenomenon

The stress equation is given by,

$$\rho \frac{\partial^2 u}{\partial^2 t} = \nabla \cdot S \tag{8}$$

$$S = S_0 + c : \left(\varepsilon - \varepsilon_o - \varepsilon_{\text{inel}}\right) \tag{9}$$

$$\varepsilon = \frac{1}{2}[\left(\nabla u\right)^T + \nabla u] \tag{10}$$

Thermal strain is given by,

$$\varepsilon_{\text{th}} = \alpha\left(T - T_{\text{ref}}\right) \tag{11}$$

The present numerical study describes the simulation of the RSW process of structural steel (AISI 1008) sheets with flat electrode tips using a 2D axisymmetric electrothermal–mechanical model in COMSOL software. The metallurgical effects are considered by the temperature dependent properties, only. Workpiece and electrode material properties are considered as a function of temperature. The electrical and thermal contact resistance at the interfaces, which plays a vital role in the process, is considered using Electrical Contact Conductance (ECC) and Thermal Contact Conductance (TCC) data. Phase change (melting/solidification) is taken into account through the latent heat capacity model. The study mainly focuses on the effect of forge (hold) time on electrode indentation and residual stresses. Also, predicted current density distribution, nugget growth, temperature variation across thickness and along the radial distance, and thermal cycles. The predicted nugget size is also compared with the measured data from the literature [7].

2.2 Numerical Model

Figure 1a shows the 2D axisymmetric model for a lap-joint of two structural steel (AISI 1008) sheets (1.52 mm thickness each) are clamped between two copper-alloy electrodes (13 mm diameter) with a flat tip (7.8 mm diameter) and a taper angle of 30°, as taken from the literature [7]. In this model, the upper electrode is considered rigid and the bottom electrode is considered rigid and constrained.

2.3 Computational Domain and Boundary Conditions

A 2D model consisting of two halves of electrodes and workpieces are considered with the necessary constraints, as shown in Fig. 1a. The electrodes are assumed to be rigid with the bottom one being constrained and grounded, while the load and electrical current are applied through top electrode. The computational domain is discretized using triangular mesh elements with a distribution, as shown in Fig. 1b. A coarse mesh is used for the electrodes with a maximum element size of 0.6 mm and a minimum size of 0.06 mm, while a fine mesh is used for the workpieces with a maximum element size of 0.12 mm and a minimum element size of 0.012 mm. It can be noted that different mesh element sizes with distribution number are being simulated for a set of process parameters and checked on the maximum temperature at the nugget centre, and accordingly the minimum and maximum element sizes with distribution number have been selected as part of the mesh independence study. A total mesh element count in the present optimum mesh is 12,926. All the edges of electrodes and workpieces outside the electrode-workpiece contact regions are assumed to be electrically insulated and exposed to the surrounding atmosphere with heat is being lost by natural convection (assumed a heat transfer coefficient of 20 W/m^{2-}K) and the ends of workpieces are clamped to avoid opening up during the RSW process. In order to maintain the rigidity of electrodes as well as to avoid overheating of its edges during the RSW process, the electrodes are water cooled [7].

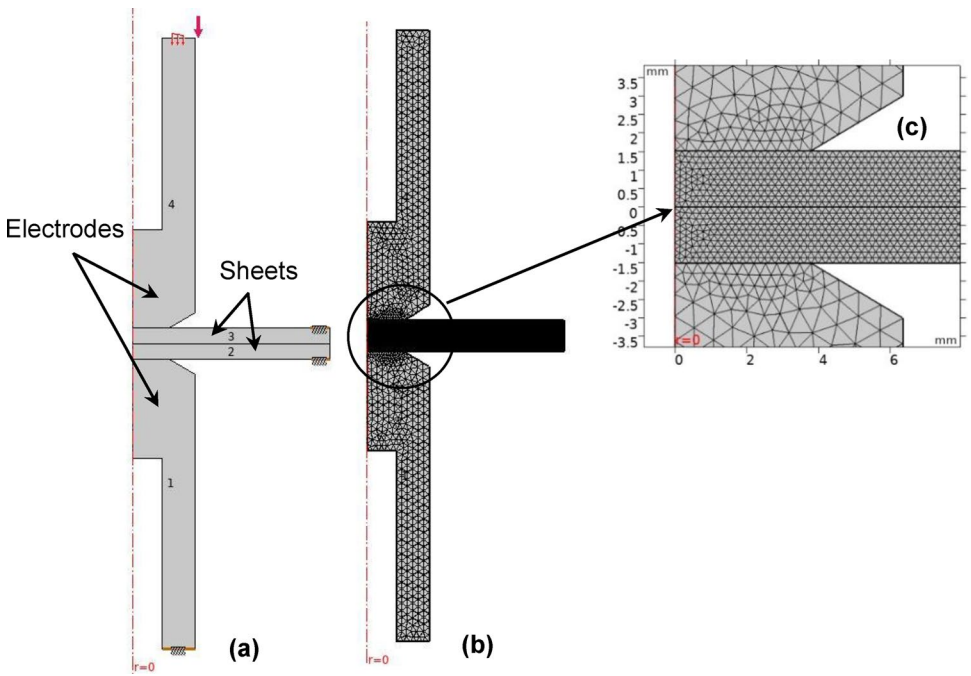

Fig. 1 **a** 2D geometry with half- electrodes and sheets **b** meshed domains **c** exploded view of meshing at E–W and W–W interfaces

2.4 Boundary Conditions

A uniform pressure and current density is applied through the top of the upper electrode, and the workpiece edges are clamped to avoid the separation of sheets during the RSW process. The bottom of the lower electrode is set as ground. The remaining surfaces are electrically insulated. The electrode is water cooled such that the inner edges are assumed to be maintained at 10 °C. The remaining surfaces of electrodes and workpieces are considered as convective heat losses (heat transfer coefficient, 20 $W/m^{2-}K$).

2.5 Process Parameters and Material Properties

In the present study, AISI 1008 steel sheets are considered for modeling and validation. The electrode material is copper-alloy. Temperature-dependent physical and mechanical properties of the materials such as thermal conductivity, electrical conductivity, specific heat, coefficient of thermal expansion, and Young's modulus are considered. Elastoplastic behavior of workpiece material is also considered. The initial yield stress of sheet material is taken as 250 MPa, and isotropic tangent modulus as function of temperature is given in Table 1. The contact resistance at the interfaces is taken into account by considering Electrical Contact Conductance (ECC) as function of temperature and Thermal Contact Conductance (TCC) is considered as constant value because its effect on nugget formation can be ignored [30]. The effect of phase change (melting/solidification) processes during the RSW process of AISI 1008 steel sheets are modeled using the latent heat capacity method [29]. The melting temperature of AISI 1008 steel is considered as 1800 K.

Figure 2 is the flowchart of a fully-coupled, electrothermal–mechanical model of the RSW process, illustrating

Table 1 Tangent modulus of AISI 1008 steel [31]

Temperature (K)	294	366	589	700	922	1033	1673
Tangent modulus (MPa)	2080	1960	1860	1690	551	68.9	6.89

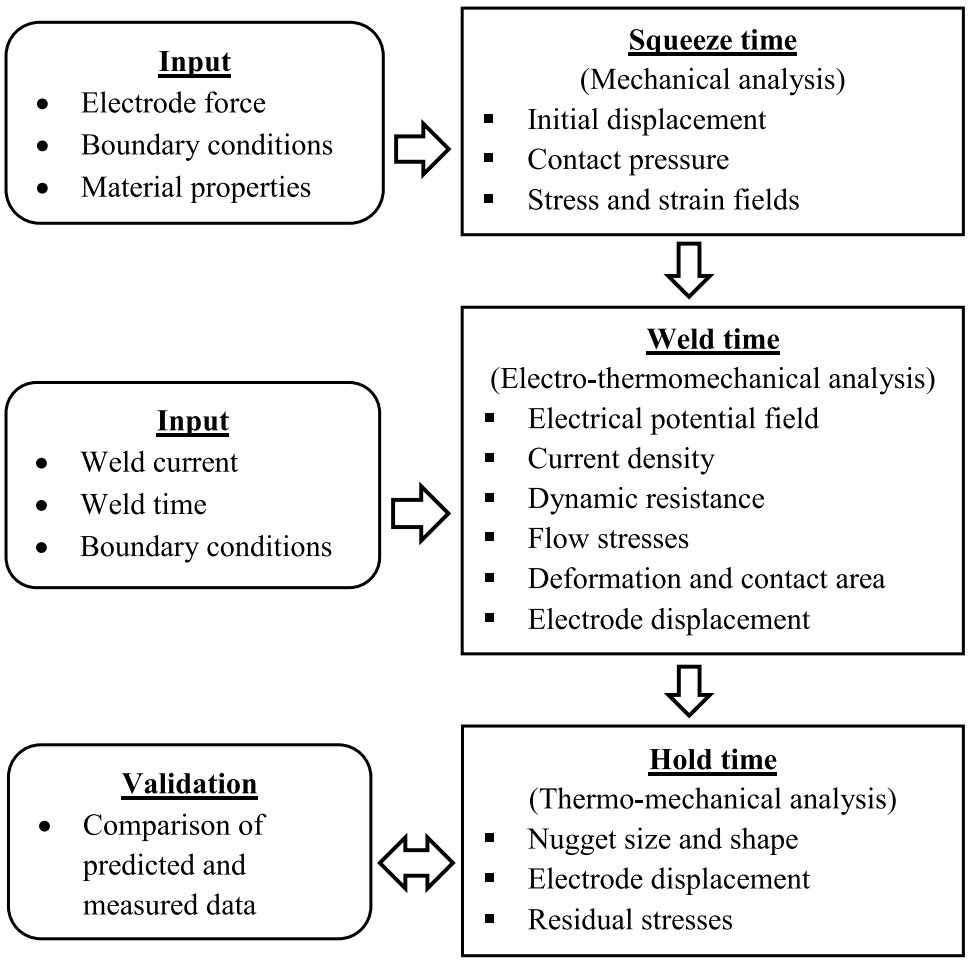

Fig. 2 Flow chart of a coupled model for RSW process with three stages and I/O parameters

three stages along with corresponding input and output parameters. The process parameters of the RSW process are load, current and weld time. In the present study alternating current (AC) having a frequency of 60 Hz [7] is used and the effect of hold time on residual stresses is extensively studied under three different conditions, as shown in Table 2.

Table 2 Process parameters used in the study [7]

Load (kN)	Current (kA)	Squeeze time (cycles)	Weld time (cycles)	Hold time (cycles)	Cooling time (cycles)
4.67	14.2	2	14	40	120
4.67	14.2	2	14	80	120
4.67	14.2	2	14	120	120

3 Results and Discussion

3.1 Current Density, Temperature and Flow Stress Distribution After Weld Stage

Figure 3 depicts the predicted distribution of current density, temperature and flow stress within the copper-alloy electrodes and AISI 1008 steel sheets (workpieces) at the end of weld time. It can be observed from Fig. 3a that the current density is more at the electrode-workpiece (E-W) interfaces with maximum being at the electrode tip radius and is due to the change in cross-sectional area (referred as edge effect). Due to the Joule heating, electrodes and workpieces are heated continuously during the weld time. However, at the interfaces more heat is being generated due to increased resistance in contrast to the bulk materials (electrode and sheets). Also, the workpieces are electrically more resistive than the electrodes and therefore more heat is generated at the workpiece-workpiece interface (W-W, referred as

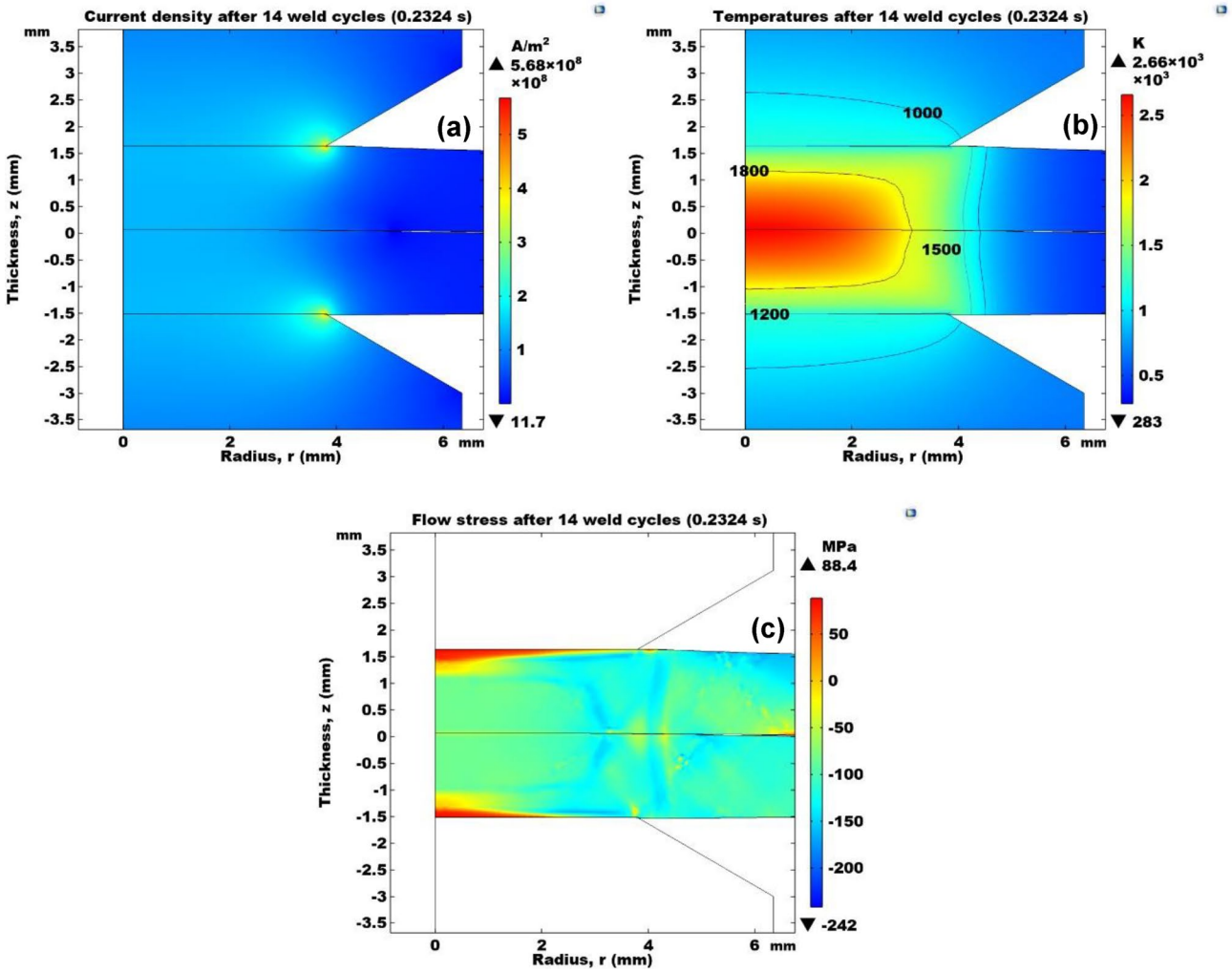

Fig. 3 After weld time, distribution of **a** current density **b** temperature **c** flow stress

faying surface) and within the workpieces. It can be noted that the area within the isothermal contour of 1800 K is the fused zone (nugget zone) with a phase change temperature of 1780 K and phase transition temperature range as 40 K, as used for phase change effect in the apparent heat capacity model. The nugget zone (NZ) at faying surface is heated maximum and is surrounded by less heated sheet material, resulting in compressive flow stresses across the NZ and tensile flow stresses at the E-W interfaces (as shown in Fig. 3c). It must be noted that the electrodes are assumed to be rigid bodies and therefore no stresses are observed (Fig. 3c). The effect of electrical and thermal resistances at the interfaces and within the bulk materials are studied in terms of the temperature variation across the electrodes at the end of weld time, as shown in Fig. 4. It is highly difficult to precisely measure the temperatures near the nugget zone during the welding process. Therefore, the simulation route is the only alternative and it provides the temperatures in real time. As expected, the maximum temperature is at the centre of nugget zone and decreases away from it both in radial and thickness (axial) directions. An accurate prediction of peak temperature along with the heating and cooling rates near the nugget zone is very important towards the solid-state phase transformation kinetics study as well as the effect of process parameters on weld quality.

3.2 Validation of Predicted Nugget Size

The nugget diameter is most commonly used parameters to relate the effect of process parameters on the weld quality. In general, larger the nugget size means higher the weld quality, and it depends on the process parameters (load, current and weld time) used. Too high current and load would have adverse effects and therefore the selection of optimum process parameters for a given sheet material and thickness is very essential. Figure 5 shows the comparison of predicted and measured [7] nugget size for the process parameters considered (given in Table 2). It can be observed that the nugget shape is elliptical due to uneven heating during the weld time because more heat is being dissipated through the coolant circulation within the electrodes. The predicted nugget diameter (major axis) and thickness (minor axis) are 6.3 mm and 2.21 mm, respectively, while the measured nugget diameter and thickness are 6.61 mm and 1.98 mm, respectively. Therefore, the error percentage in nugget diameter (~4.7%) and thickness (~11.9%) could be partly due to the assumption of constant thermal contact conductance (TCC) data at the interfaces and partly due to neglect of melt flow dynamics by the Lorentz force effect. The later one may have a significant effect on the nugget thickness as well as the overall shape [30].

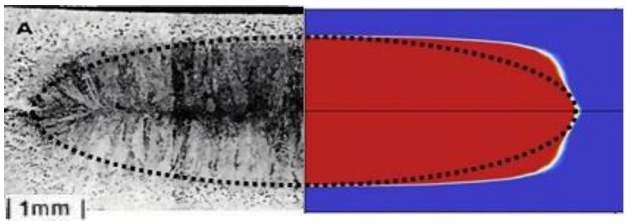

Fig. 5 Comparison of measured and predicted nugget geometry after weld time (14 cycles)

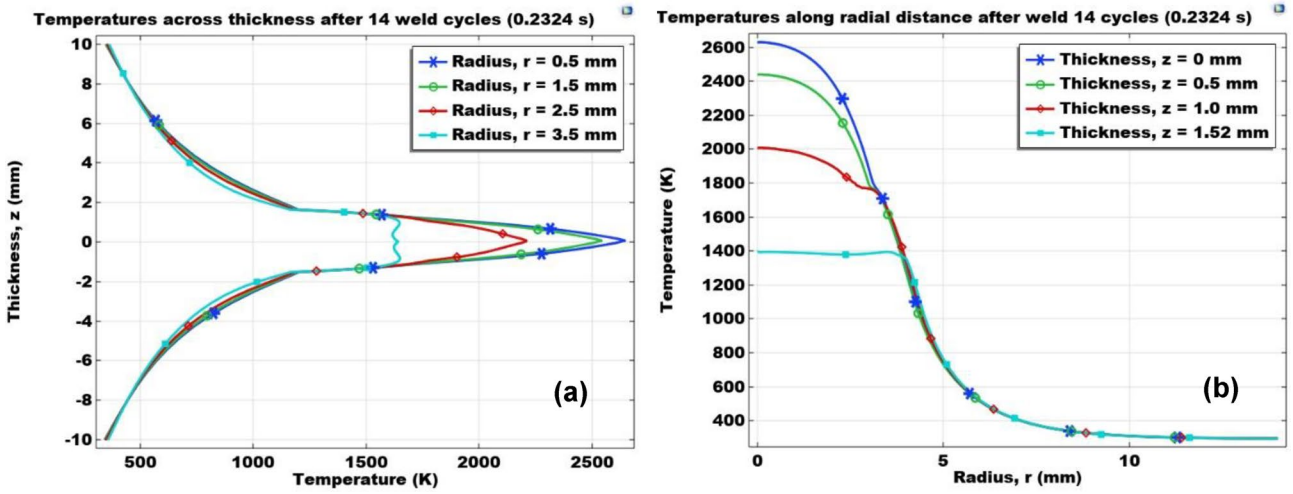

Fig. 4 After weld time, **a** temperature variation across thickness and at different radii **b** temperature variation along radial distance and at different thickness

3.3 Residual Stresses After Forge (Hold) and Cooling Stages

The structural stability of RSWed joint depends on the nugget size as well as the residual stresses. In general, the residual stresses are tensile in the nugget centre and compressive away from it. But, the stresses must be minimum for which solidification of the nugget must be done under the electrode load (forged condition). From the literature, present authors learnt that a hold time of 20–30 cycles are typically used for thin sheet metals, irrespective of the type of metal and coolant mechanism used. In the present study, different hold times are being explored to study its effect on the temperatures and residual stresses. Figure 6 depicts the distribution of predicted temperatures and residual stresses after different hold times (40, 80 and 120 cycles), keeping the squeeze time (2 cycles) and weld time (14 cycles) fixed. It can be clearly observed that the temperatures near the nugget zone have come down very significantly from a hold time of 40 cycles to 120 cycles, and is due to continuous heat dissipation to the coolant through the highly conducting copper-alloy electrodes (heat sink). Also, the maximum residual stress (290 MPa) after a hold time of 40 cycles is found to be above the base metal yield stress (250 MPa) and therefore requires further cooling of sheets by ambient air (i.e., natural convective cooling). To study the effect of forge (hold) time on the residual stresses across the nugget zone, simulations are performed with three different sets—40 hold cycles and 120 cooling cycles (h40–c120), 80 hold cycles and 120 cooling cycles (h80-c120) and 120 hold cycles and 120 cooling cycles (h120–c120). Figure 7 depicts the distribution of temperatures and residual stresses at the end of cooling time with three different hold times (40, 80 and 120 cycles), as mentioned above. It is expected that increasing the hold time cools down the sheets to low temperatures, which in turn influences the final residual stress distribution. It must be noted that during hold time, coolant is passed through the electrodes and therefore more heat is being dissipated with increase in hold time. During the cooling time, the electrodes are disabled and the natural air cooling of sheets results in redistribution of temperatures as well as residual stresses. It can be clearly observed from Figs. 7b, d, f that the final residual stresses across the nugget zone decreases significantly with increase in hold (forge) time. Also, more of compressive residual stresses are developed with increase in hold time due to prolonged forged cooling of sheets.

Development of stresses during the RSW process is quite complex due to high heating and cooling rates besides the mechanical load acting on the sheets. In order to understand the redistribution of flow stresses in the subsequent cooling (hold time), a point to point variation of stresses along the faying surface and on the sheet top surface are examined at the end of different stages with a primary focus being on the effect of different hold (forge) times on the final residual stresses. Figure 8 depicts the variation of flow stresses (after weld time) and residual stresses (after hold plus cooling times) along the faying surface (Fig. 8a, c, e) and on the sheet top surface (Figs. 8b, d, f). The thermal and flow stress fields at the end of weld time is common for subsequent hold and cooling times, but different hold times (40, 80 and 120 cycles) are being considered. It can be observed that the flow stresses (due to heating) are compressive across the nugget zone. Subsequent hold time during which the nugget zone cools down under the electrode load followed by cooling time results in redistribution of compressive stresses into tensile in the nugget zone and compressive away from it. Redistribution of residual stresses with reduced values across the nugget zone are clearly observed at the faying surface as well as the sheet top surface. Also, the transition of tensile residual stresses along the faying surface to compressive residual stresses is clearly observed with the optimum hold time. Therefore, it is suggested that the nugget zone must be cooled under the forged condition (electrode load active) such that the residual stresses would be minimum. The minimum time to attain the lowest residual stresses at the faying surface may be considered as the optimum hold (forge) time. Figure 9 shows the final residual stress variation along the faying surface and on the sheet top surface, considering different hold times (40, 80 and 120 cycles) followed by additional cooling time (120 cycles, fixed). It can be clearly observed that a weld schedule with 40 cycles of hold time results in high and mixed residual stresses in the nugget, while with 80 cycles of hold time a reduced and tensile residual stress in the nugget zone. With a hold time of 120 cycles, the tensile residual stresses are minimum in the nugget zone and also a transition to compressive residual stresses in the heat-affected zone, which is in agreement with the experimental findings from the literature [25]. In overall, the residual stresses (tensile and compressive) decrease with increase in hold (forge) time, and is desirable as it increases the fatigue life of the joint.

3.4 Thermal Cycles After Hold Stage

Figure 10 depicts the thermal cycles at selected locations from the nugget center ($r=0$, $z=0$) and within the top sheet for weld time (heating) and hold time (cooling). It can be clearly observed that the peak temperature as well as heating and cooling rates are high at the nugget center and decreases away from it. In Fig. 10a, b, the thermal cycles within the nugget (fused) zone clearly shows the effect of phase change through the apparent heat capacity method used in the present coupled model. During the phase change (melting and solidification) process, the heating and cooling curves are nearly flat.

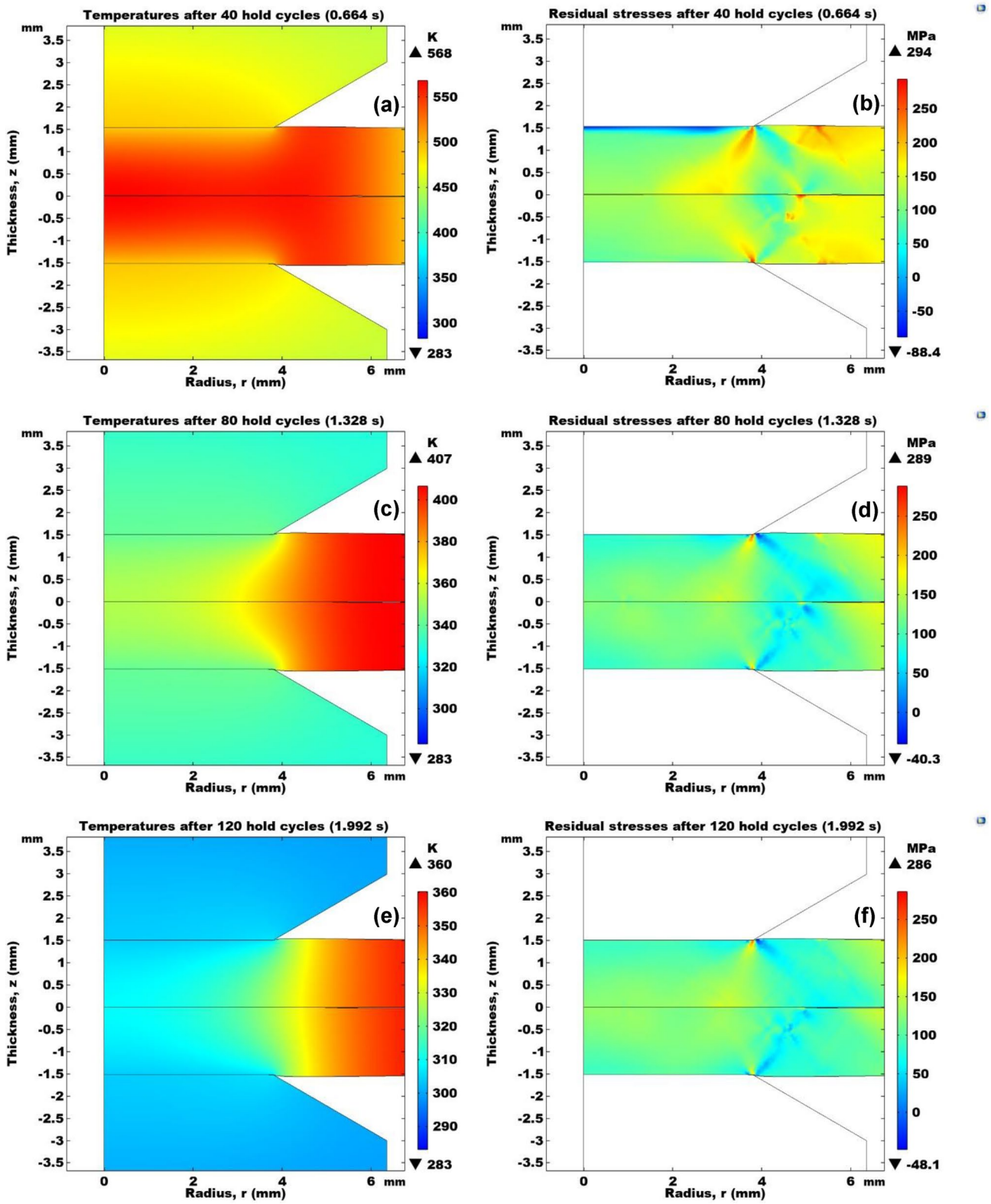

Fig. 6 Distribution of **a**, **c**, **e** temperatures **b**, **d**, **f** residual stresses, after different hold times (40, 80 and 120 cycles). Weld time (14 cycles) and cooling time (120 cycles) are fixed

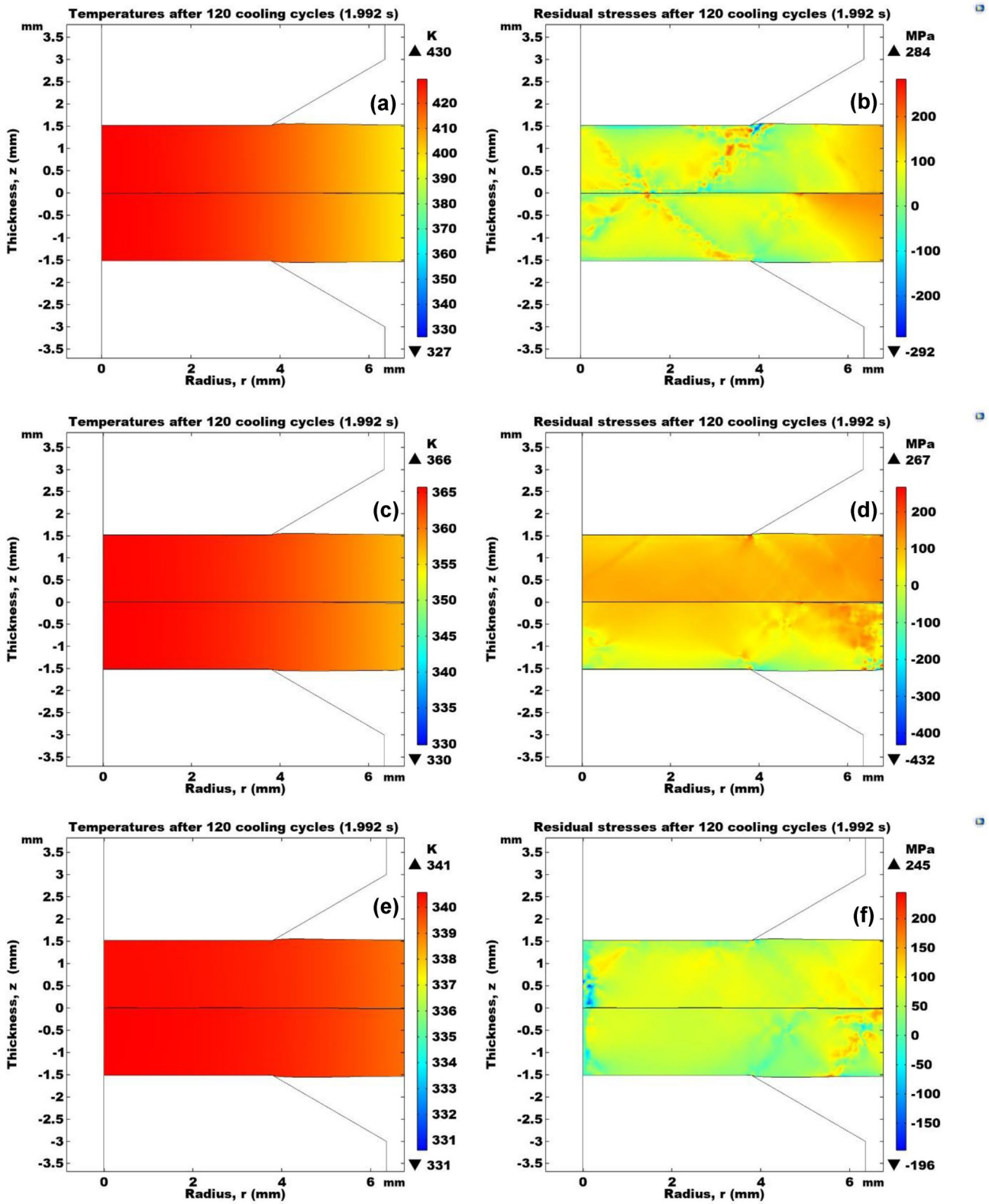

Fig. 7 Distribution of **a**, **c**, **e** temperatures **b**, **d**, **f** residual stresses, after a weld schedule with different hold times (40, 80 and 120 cycles). Weld time (14 cycles) and cooling time (120 cycles) are fixed

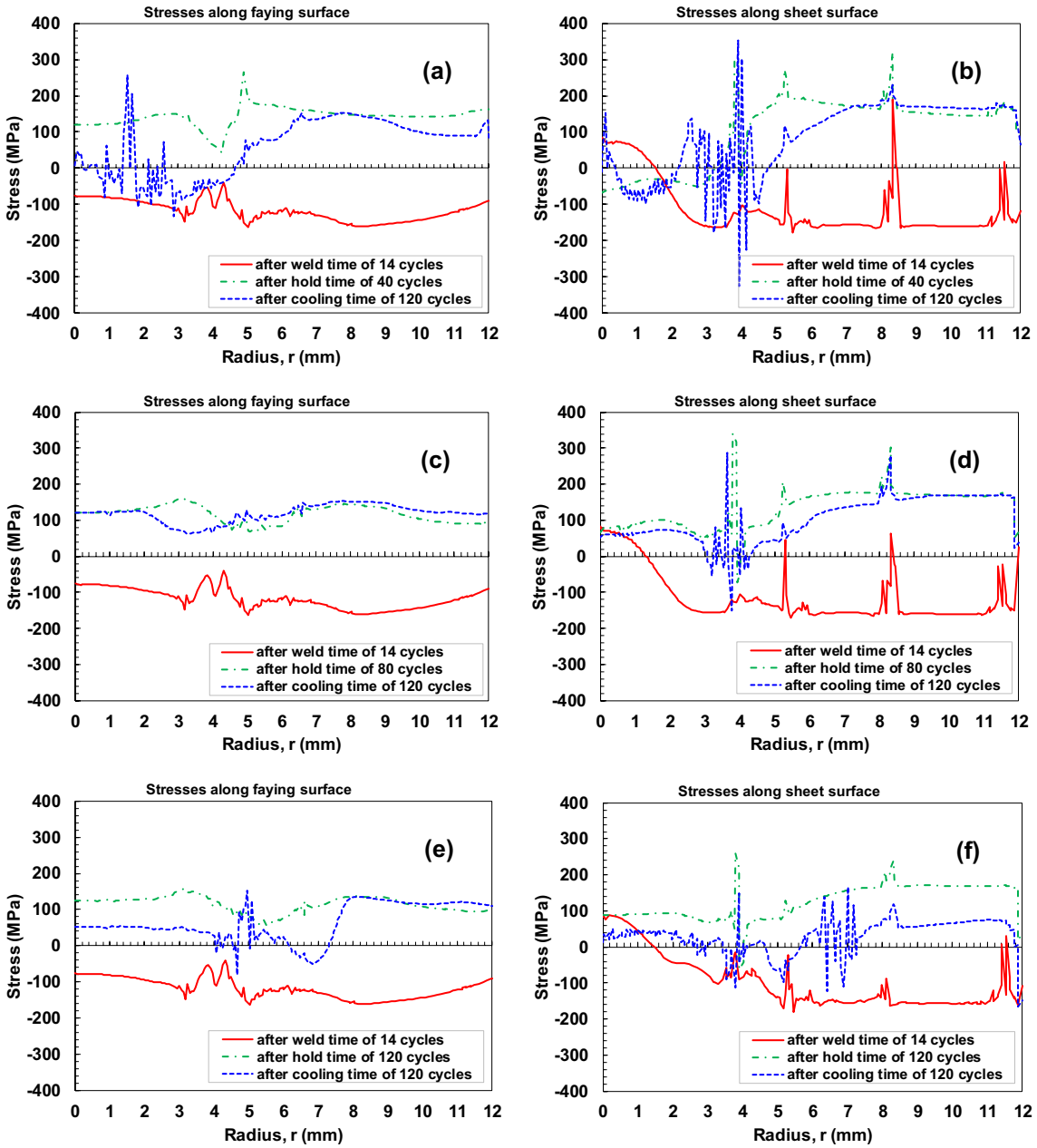

Fig. 8 Spatial stress variation after different stages with different hold times (40, 80 and 120 cycles); **a**, **c**, **e** along faying surface **b**, **d**, **f** along top sheet surface

3.5 Electrode Displacement and Workpiece Deformation

Electrode displacement during the RSW process is one of the important parameters used for in-line process monitoring and control of process parameters towards achieving increased quality. Further, the electrode indentation on the sheets after the welding is an indication of fusion at the faying surface and hence the formation of nugget. Therefore, it is important to confirm by the coupled model on the optimum weld schedule (consisting of squeeze, weld and hold times) by studying the electrode displacement as well as the deformation of sheets (workpieces) during the process. Figure 11 depicts the electrode displacement during three weld schedules with different hold times. It can be noted that during squeeze time, the electrode displaces downward (− 0.0014 mm) however small it is, then displaces upward during the weld time (0.119 mm) due to heating and expansion of sheets and finally displaces downward during the hold time due to cooling and contraction of the sheets.

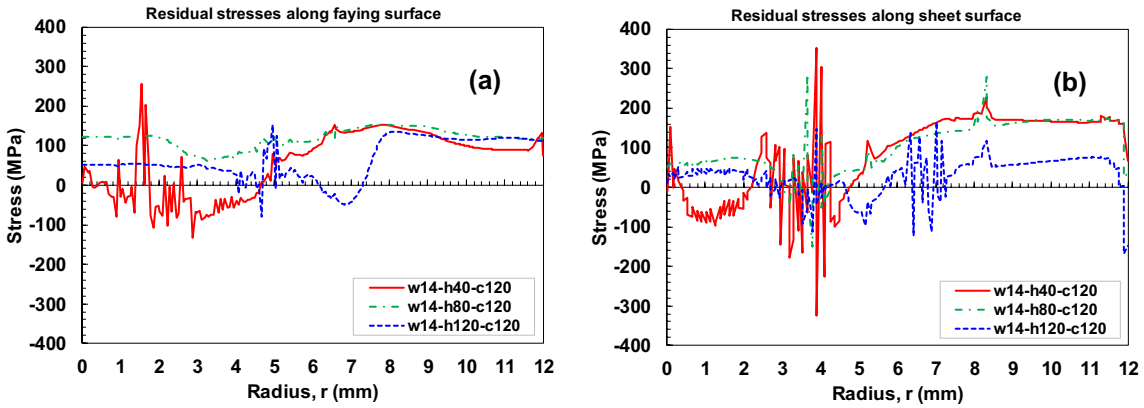

Fig. 9 Residual stress variation with different hold times (40, 80 and 120 cycles); **a** along faying surface **b** along top sheet surface

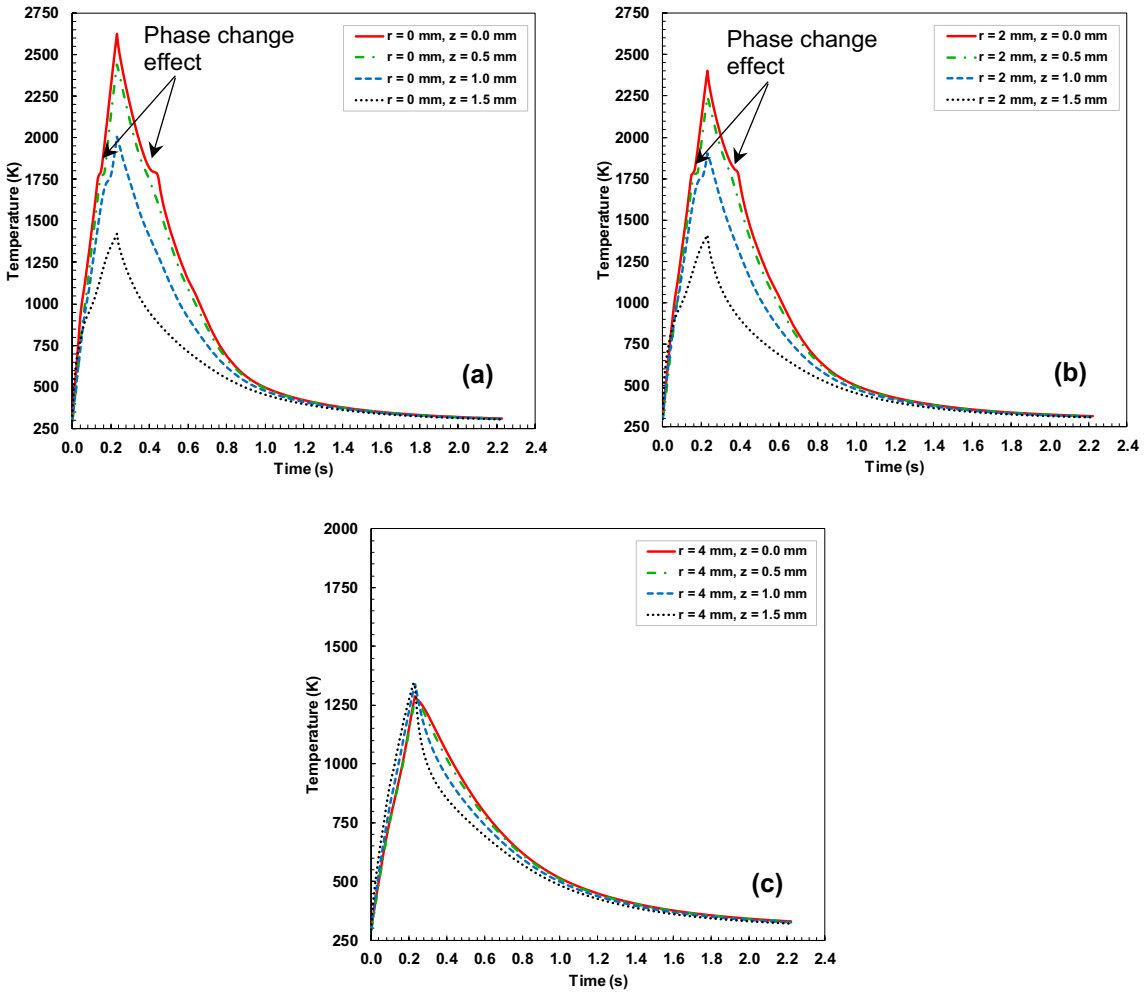

Fig. 10 Thermal cycles at selected locations (r, z) within the top steel sheet for a weld schedule of 14 weld cycles, 120 hold cycles and 120 cooling cycles

It can be clearly observed in Fig. 11 that the weld schedule with a hold time of 80 and 120 cycles show the indentations (− 0.008 mm and − 0.015 mm, respectively) and it asymptotically increases with increase in the hold time. Therefore, it can be concluded from the electrode displacement profile that for the process parameters (load, current

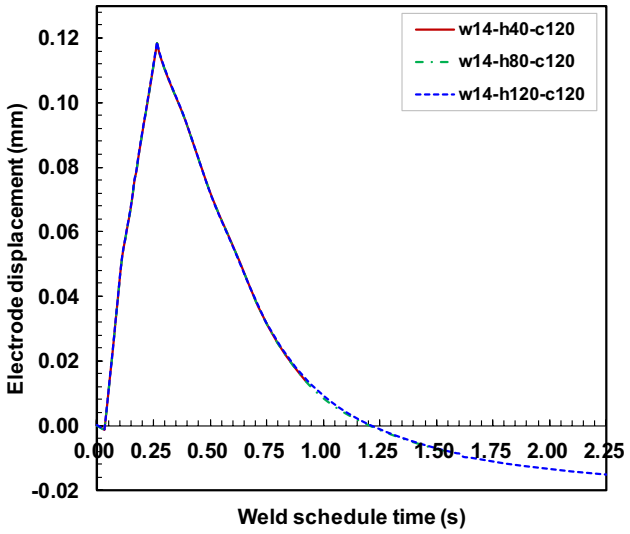

Fig. 11 Electrode displacement positions during different weld schedule times

and weld time) considered, the minimum hold time required is around 120 cycles. Figure 12a depicts the deformed states of sheets in radial distance (i.e., along sheet length) during the weld time (14 cycles), while Fig. 12b during the hold time (120 cycles). It can be observed that the maximum upward displacement of the sheet (bulging effect) at the end of weld time is 0.119 mm and a maximum downward displacement underneath the electrode (i.e., indentation) at the end of hold time is 0.015 mm, which are in complete agreement with the electrode displacement profile. Further, the sheet metal adjacent to the electrode is free to expand (maximum upward displacement after 14 weld cycles) and contract (final upward displacement after 120 hold cycles) is in accordance with the conservation of mass of the sheet material.

In overall, the developed coupled model considering the temperature dependent properties, contact conductance model and apparent heat capacity model is able to predict several important parameters, which helps to design optimum process parameters as well as to design the algorithms for control systems (electrical and mechanical), which are otherwise highly difficult to precisely measure during the RSW process.

4 Conclusions

A 2D axisymmetric coupled electro-thermomechanical model has been developed in COMSOL Multiphysics software by considering the elastoplastic behaviour of AISI 1008 steel sheets, contact conductance models for contact resistances at interfaces and apparent heat capacity model for phase change effects during the Resistance Spot Welding (RSW) process. Subsequently, for a given electrode load (4.67 kN), weld current (14.2 kA) and weld time (14 cycles), the effect of different hold times (40, 80, 120 cycles) followed by the natural air cooling time (120 cycles) has been studied on the distribution of temperatures and residual stresses, electrode displacement and sheet metal deformation. The following important observations are drawn from the simulations;

(i) After weld time, maximum temperatures found to be at the interfaces (workpiece-workpiece and electrode-workpiece) in contrast to the bulk materials (workpieces and electrodes). Also, flow stresses are compressive across the nugget zone.
(ii) Peak temperature, heating and cooling rates depend on the location from nugget centre, with maximum values being at the faying surface (W/W interface) and decreases away from it.

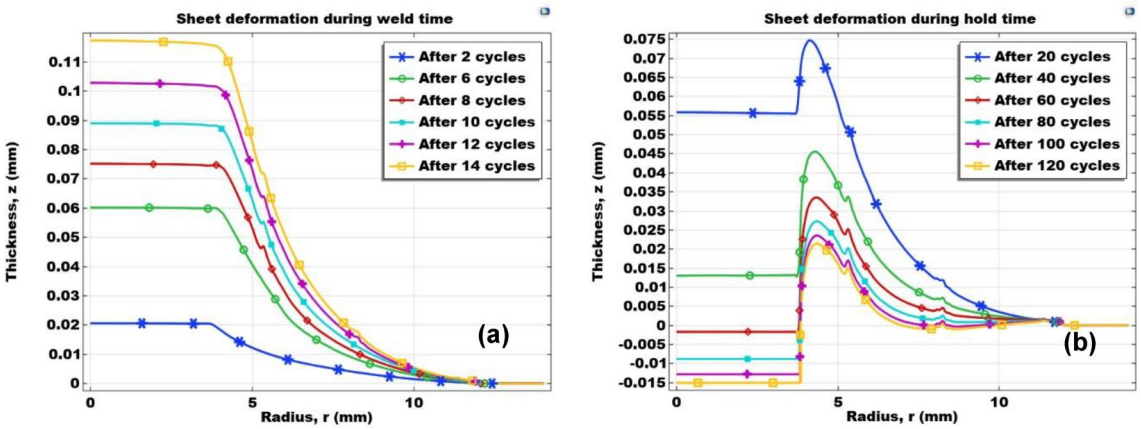

Fig. 12 Sheet deformation and displaced positions along radial distance during **a** weld time **b** hold time

(iii) Predicted and measured nugget size and shape are in close agreement. However, there is a scope for improvement with the melt flow dynamics (not considered in the present study).
(iv) Residual stresses (tensile and compressive) decreases with increasing hold (forge) time, with tensile stresses in nugget zone (NZ) and compressive stresses in heat-affected zone (HAZ).
(v) Optimum hold time must be used to minimize the residual stresses and to have a minimum indentation on sheets, an indication of nugget formation.
(vi) Coupled model predictions on nugget size, residual stresses and electrode displacement helps to study the weld quality without making actual welds and tedious material testing and characterization done.

Authors Contribution: JJ, PK RG: Conceptualization, simulations, analysis, validation, manuscript writing and editing. JJ, VG, SKP, SP: Administration and supervision.

Funding This research did not receive any specific grant from funding agencies in the public, commercial, or not-for-profit sectors.

Declarations

Conflict of interest The authors declare no conflict of interest.

References

1. Pouranvari M, *Arch Metall Mater* **58** (2013) 67. https://doi.org/10.2478/v10172-012-0152-y
2. Mirzaei F, Ghorbani H, and Kolahan F, *Int J Adv Manuf Tech* **92** (2017) 3489. https://doi.org/10.1007/s00170-017-0407-x
3. Rao S S, Arora K S, Sharma L, and Chhibber R, *Trans Indian Inst Met* **74** (2021) 1419. https://doi.org/10.1007/s12666-021-02237-2
4. Aydin K, Hidiroglu M, and Kahraman N, *Trans Indian Inst Met* **75** (2022) 1279. https://doi.org/10.1007/s12666-021-02482-5
5. Raath N D, Norman D, Mcgregor I, Dashwood R, and Hughes D J, *Metall Mater Trans A* **48** (2017) 2900. https://doi.org/10.1007/s11661-017-4079-9
6. Ao S, Li C, Huang Y, and Luo Z, *Measurement* **161** (2020) 107892. https://doi.org/10.1016/j.measurement.2020.107892
7. Gould J E, *Weld J* **66** (1987) 1s.
8. Tsai C L, Dai W L, Dickinson D W, and Papritan J C, *Weld J* **70** (1991) 339s.
9. Gupta O P, and De A, *Trans ASME J Manuf Sci Eng* **120** (1998) 246. https://doi.org/10.1115/1.2830120
10. Babu S S, Santella M L, Feng Z, Riemer B W, and Cohron J W, *Sci Technol Weld Join* **6** (2001) 126. https://doi.org/10.1179/136217101101538631
11. De A, *Sci Technol Weld Join* **7** (2002) 119. https://doi.org/10.1179/136217102225002998
12. Hou Z, and Kim III-Soo, Wang Y, Li C, Chen C, *J Mater Process Technol* **185** (2007) 160. https://doi.org/10.1016/j.jmatprotec.2006.03.143
13. Moshayedi M, and Sattari-Far I, *J Mater Process Technol* **214** (2014) 2545. https://doi.org/10.1016/j.jmatprotec.2014.05.008
14. Wang B, Hua L, Wang X, Song Y D, and Liu Y, *Int J Adv Manuf Tech* **83** (2016) 1917. https://doi.org/10.1007/s00170-015-7703-0
15. Lee Y, Jeong H, Park K, Kim Y, and Cho J, *J Mech Sci Technol* **31** (2017) 3455. https://doi.org/10.1007/s12206-017-0634-y
16. Hamedi M, and Atashparva M, *Weld World* **61** (2017) 269. https://doi.org/10.1007/s40194-016-0419-4
17. Guan S, He X, Wang X, and Hua L, *Int J Adv Manuf Tech* **110** (2020) 79. https://doi.org/10.1007/s00170-020-05809-6
18. Chino T, Kunugi A, Kawashima T, Watanabe G, Can C, and Ma N, *Materials* **14** (2021) 7180. https://doi.org/10.3390/ma14237180
19. Brizes E, Jaskowiak J, Abke T, Ghassemi-Armaki H, and Ramirez A J, *J Mater Process Technol* **297** (2021) 117276. https://doi.org/10.1016/j.jmatprotec.2021.117276
20. Reddy Gillela P K, Jaidi J, Gude V, Pathak S K, and Srivastava D, *Numer Heat Transf A: Appl* **82** (2022) 1. https://doi.org/10.1080/10407782.2022.2105088
21. Nodeh I R, Serajzadeh S, and Kokabi A H, *J Mater Process Technol* **205** (2008) 60. https://doi.org/10.1016/j.jmatprotec.2007.11.104
22. Dalewski R, Jachimowicz J, and Pietrzakowski M, *J Thermal Stresses* **33** (2010) 843. https://doi.org/10.1080/01495739.2010.482370
23. Iyota M, Mikami Y, Hashimoto T, Taniguchi K, Ikeda R, and Mochizuki M, *J Phys Conf Ser* **379** (2012) 012051. https://doi.org/10.1088/1742-6596/379/1/012051
24. Wan X, Wang Y, and Zhang P, *Int J Adv Manuf Tech* **92** (2017) 2619. https://doi.org/10.1007/s00170-017-0191-7
25. Moharrami R, and Hemmati B, *J Manuf Processes* **27** (2017) 284. https://doi.org/10.1016/j.jmapro.2017.05.007
26. Prabitz K, Pichler M, Antretter T, Schubert H, Hilpert B, Gruber M, Sierlinger R, and Ecker W, *Materials* **14** (2021) 5411. https://doi.org/10.3390/ma14185411
27. Khanna S K, and Long X, *Sci Technol Weld Join* **13** (2008) 278. https://doi.org/10.1179/174329308X283884
28. De A, and DebRoy T, *Sci Technol Weld Join* **16** (2011) 201. https://doi.org/10.1179/136217111X12978476537783
29. Heat Transfer Module User's Guide, COMSOL 5.4, Chapter 4, pp. 175. https://doc.comsol.com/5.4/doc/com.comsol.help.heat/HeatTransferModuleUsersGuide.pdf
30. Li Y, Lin Z, Shen Q, and Lai X, *ASME J Manuf Sci Eng* **133** (2011) 1. https://doi.org/10.1115/1.4004319
31. Wang J, Wang H P, Lu F, Carlson B E, and Sigler D R, *Int J Heat Mass Transf* **89** (2015) 1061. https://doi.org/10.1016/j.ijheatmasstransfer.2015.05.086